Shap. Mem. Superelasticity
https://doi.org/10.1007/s40830-024-00474-0

ORIGINAL RESEARCH ARTICLE

The Development of a 2D Numerical Model of a Device Using the Elastocaloric Effect to Cool Electronic Circuits

Luca Cirillo[1] · Adriana Greco[1] · Claudia Masselli[1]

Received: 11 October 2023 / Revised: 8 January 2024 / Accepted: 19 January 2024
© The Author(s) 2024

Abstract The scientific community has been working hard lately to develop fresh, environmentally friendly refrigeration technologies. Those based on solid-state refrigerants are among the Not-In-Kind Refrigeration Technologies that show great promises. The one based on the elastoCaloric Effect is among the most interesting of them. This paper presents the development of a 2D numerical model for a device harnessing the elastocaloric effect with the primary objective of cooling electronic circuits. The study focuses on the intricate interplay between mechanical and thermal aspects, capturing the dynamic behavior of the elastocaloric material in response to cyclic mechanical loading. The numerical model incorporates detailed descriptions of the electronic circuits, accounting for heat dissipation and thermal management. Through simulations, the optimal configuration for efficient cooling is explored, considering various operative conditions and mechanical loading conditions (tensile and bending). The findings contribute to the advancement of elastocaloric cooling technology, offering insights into the design and optimization of devices aimed at enhancing electronic circuit performance through effective thermal control. The results that the most promising configuration is based on bending, a design choice resulting appropriate for cooling the electronic circuits.

This invited article is part of a special topical focus in *Shape Memory and Superelasticity* on Elastocaloric Effects in Shape Memory Alloys. The issue was organized by Stefan Seelecke and Paul Motzki, Saarland University.

✉ Claudia Masselli
claudia.masselli@unina.it

[1] Department of Industrial Engineering (DII), University of Naples Federico II, Piazzale Tecchio 80, 80125 Naples, Italy

Keywords Stress-induced martensitic transformation · Mechanical behavior · NiTi materials · Austenite · Martensite · Shape memory · SMA

Introduction

General Concepts

More than 20% of overall energy usage is made up of refrigeration and air conditioning. The most popular cooling method nowadays is Vapour Compression (VC), which is not environmentally friendly due to the usage of refrigerants that contribute to the greenhouse effect and because its technological capabilities have been achieved. This explains why the scientific community is interested in creating novel, non-conventional refrigeration technologies. Among them there are solid-state refrigeration-based technologies that benefit from: (i) use of solid refrigerants with no direct greenhouse effect, since zero is their Global Warming Potential (GWP); (ii) energy performance potentially up to +50 + 60% than VC systems [1]. The caloric effect of solid-state refrigerants manifests itself as a temperature variation of the caloric material in an adiabatic transformation changing the intensity of the applied field. In the solid-state refrigeration technologies one of the most promising is that based on elasto-Caloric Effect (eCE) [2]. Shape Memory Alloys (SMA) are used as solid refrigerants and exhibit superelasticity and the shape memory phenomenon, meaning that they may return to their original shape after being stressed or relaxed. A SMA can exist in the structural states of austenite and martensite, and the transition from one state to the other can also be obtained by the loading and the unloading process [3].

The elastoCaloric (eC) SMAs' above-mentioned behavior enables the design of two different thermodynamic cycles.

Published online: 11 March 2024

The direct thermally driven cycle, which could be used in a heat engine, and the inverse stress-driven cycle, which could be used in a cooling or heating pump system. In many well-known thermodynamical cycles, the inverse stress-driven cycle can be used to influence how a cooling system behaves [4]. The reverse Brayton-based AeR cycle, also known as the Active elastocaloric Regenerative refrigeration (AeR) cycle, is the most used eC refrigeration cycle. The elastocaloric SMA also serves as a means of regeneration in an AeR-based system, and a secondary fluid acts as a means of heat transfer. Regeneration allows for the recovery of heat that would otherwise be lost in a single stage cycle. As a result, the AeR cycle can ensure that the temperature spread across the regenerator is bigger than the adiabatic temperature jump (ΔT_{ad}), which belongs exclusively to eCE and to the material itself, it is defined as the temperature change that occurs when the elastocaloric material undergoes adiabatic deformation, i.e., deformation without heat exchange with the external environment. The maximum temperature span that can be detected in the regenerator without regeneration is capped by the ΔT_{span}.

When the elastocaloric material is loaded, its temperature rises; next, a Heat Transfer Fluid (HTF) is crossed over it to release heat; next, it is unloaded, causing its temperature to drop and finally, a cold HTF is crossed over it to absorb heat from the thermal load. The benefits of elastocaloric refrigeration include: (1) readily available and inexpensive refrigerant materials; and (2) ease of delivering a mechanical field of high intensity to the material.

State of the Art

Ten years ago, elastocaloric refrigeration came into the public eye. Since then, scientists have concentrated their efforts on developing the devices and finding new promising materials that are appropriate for cooling and heat pumping. Additionally, modeling is important because it is linked to the branch of device realization and aids in optimization.

a) Nickel Titanium is the benchmark elastocaloric substance that has been investigated and used the most. Even if it can withstand up to 9% strain, the binary alloy contacts 25.5 K and 17 K for 5% strain (loading and unloading) [5, 6]. The binary alloy also has other benefits, such as strong shape memory qualities, widespread market availability, and a tolerable fatigue life for eC applications. The latter is essential since a material with a short fatigue life has a short service life. Hysteresis can be reduced or the fatigue life can be improved with the aid of Ni–Ti alloys made of three or four components [7]. Chluba et al. investigated and showed in 2015 [8] that the addition of Cu to Ni–Ti alloys can offer up to 10^7 cycles of loading and unloading before cracks emerge. Due to their cheaper prices and potential for eCE to develop under stress values lower than those for NiTi-based alloys, Cu- and Fe-based alloys were also used in eC procedures. The greatest ΔT_{ad} reported for the Fe-based alloys is 5 K, while the highest ΔT_{ad} detected in Cu-alloys is 15 K under 130 MPa of stress. Shape Memory Polymer (SMP) is a new class of elastocaloric materials that also includes natural or synthetic rubbers [9–11]. The rubbers' biggest drawback is the extreme elongation required for eCE manifestation (strain up to 600% of the unloaded length).

b) To the best of our knowledge, there have been slightly more than fifteen elastocaloric devices created in laboratories up to the year 2023 [12]. Some of these devices experiment with the AeR cycle, while others use the solid-to-solid cycle. While some of them are rotary, some of them are forced by linear drives. Cui et al. [13] unveiled the first eC prototype in 2012; it was a rotating device made of two rings through which NiTi wires were fastened. The maximum temperature span (ΔT_{span}) recorded was 17 K but, due to the device's design, the lifetime of the refrigerant was severely constrained by how easily cracks might form. Greco et al. and Kabirifar et al. [12, 14] examined the eC devices developed in 2019. Interesting among them was a rotary system [15] that uses the quaternary alloy $Ni_{45}Ti_{47.25}Cu_5V_{2.75}$ to extend the life of the materials. Other smaller size elastocaloric devices were created in addition to the previously stated devices that were focused on air conditioning or heat pumps. The bridge system created by Bruederlin et al. [16] is noteworthy since it does not require HTF because a slice of elastocaloric material is loaded through bending while also being transported up and down. The device was subsequently upgraded [17] by using a TiNiFe slice as the refrigerant. Through the cyclical stretching of a few Ni-Ti wires, the microscale cooler developed by Snodgrass and Erickson [18] in 2019 demonstrated the largest temperature span (28.9 K). In parallel, Ossmer et al. [19] demonstrated a miniature elastocaloric cooler that could produce 2.9 W g^{-1} of cooling power and 3.2 of coefficient of performance (COP).

The most recent elastocaloric devices were presented in 2022 by Xi'an Jiaotong University [20], University of Ljubljana [21], Technical University of Denmark in collaboration with the German Fraunhofer Institute for Physical Measurement Techniques [22], and University of Maryland [23]. Materials from the binary NiTi alloy with a variety of compositions are employed as elastocaloric refrigerants. The greatest temperature span of the Chinese prototype [20] is 9.2 K and it uses air as the heat transfer fluid. The other three, where water circulates as HTF, are all compression-loading based. The Slovenian device [21] (mounting tubes of $Ni_{55.8}Ti_{44.2}$) reached the maximum temperature span of 31.3 K, which is the highest value ever at best we know. On the other hand, the DTU device's [22] peculiarity is to demonstrate a promising 1071 W kg^{-1} as specific cooling power, determined by using $Ni_{56.25}Ti_{43.75}$ tubes in an AeR cycle. The University of Maryland's prototype [23] is a

linear alternate mounting of a staggered $Ni_{50.5}Ti_{49.5}$ tube. The highest temperature range that has been observed is 16.6 K, however no information regarding cooling power or COP has yet been provided.

In 2022 the group of University of Naples Federico II introduced a hydraulic-driven rotary elastocaloric device [24]. The elastocaloric material is shaped as 600 wires (diameter 0.5 mm and length 300 mm) arranged in the annular section between two concentric cylinders (internal radius of 120 mm, an external radius of 135 mm, and a length of 300 mm). A maximum COP of 6.22 (corresponding to a second law analysis efficiency of 60%) was evaluated under an airflow speed of 6 m s^{-1} and a frequency of 0.3 Hz, corresponding to a utilization factor of 0.44. 28.5 K and 5400 W kg-1 are the reached peaks of temperature span and cooling power [25, 26].

One can see from the state of the art that there are still many steps to be done before an elastocaloric device can be produced on a wide scale. One of the causes is the lifespan of the devices as a whole and the eC materials used. The many studied and investigated areas of application for eC technology are refrigeration and air conditioning.

The short fatigue life of the eC materials combined with the type of applied stress (to make eCE manifest in the AeR cycle) as well as the achievement of optimal operational conditions is the bottleneck of the eC technology. Modeling allows for the optimization of the device's dimensions and operational circumstances. With the exception of the models created by Cirillo et al. [27], where a group of wires was two-dimensionally studied, the majority of eC models established are 1D [28].

Regarding the type of loading used, it is unavoidable that cracks may develop over time due to the mechanical solicitations the material is subjected to throughout the cycles of loading and unloading. Xu et al have deeply reviewed tension-compression pro and cons of NiTi alloys [29] The crack growth that occurs during loading and unloading cycles is a drawback of tension. Cycles of SMA trainings before employment can improve the resistance to fatigue life of NiTi alloys [2, 30]. Compression has the drawback of reducing the amount of available heat transfer surface [31]. Although there have been several studies on the fatigue life of SMAs (mainly the binary NiTi alloy) under tension, there have been far fewer investigations on the same issue under compression. Studies, for instance, demonstrate that a durable operation (10^5 cycles) can be accomplished in the NiTi alloy with strains of around 2%, which translates to a comparatively tiny ΔT_{ad}. With the potential to attain up to 70 million loading/unloading cycles, the first investigations on NiTi cylinders and cubes under compression revealed a considerable improvement compared to tension [32, 33]. In addition, a recent study [34] focused on torsion as an alternative to compression and tension, showing a substantial increase in the material's lifetime even with a smaller amount of adiabatic temperature change. It appears that bending is a good solution for both the issue of cracks and acceptable temperature variations. According to Sharar et al. [35], axisymmetric bending permits a fivefold decrease in the force needed for similar COP and temperature span, which directly translates to a decrease in the size, weight, and power input needed for eC cooling systems. These advantages of loading by bending can all be seen as a promising way to get over some of the major obstacles that elastocaloric system realization faces.

Aim of the Investigation

CHECK TEMPERATURE is the acronym of "Controlling the Heating of Electronic Circuits: a Key-approach Through Elastocaloric Materials in a Prototype Employing them as Refrigerants of an AcTive Ultrasmall Refrigerator". In order to cool electrical circuits, the CHECK TEMPERATURE project aims to create the first elastocaloric device customized for this purpose. The plan has been to create a device based on the AeR as the thermodynamic cycle and bending as the loading/unloading mode, even if it is small-scale and unlike the ones that already exist.

The purpose of this study is to provide the findings of a numerical analysis used to build the CHECK TEMPERATURE prototype, which involved optimizing both the working environment and the geometrical configuration for the assembly of the elastocaloric material in the channel.

The following are the primary novelties in this paper:

- The area of application. In reality, the cooling of electronic circuits is an intriguing yet unexplored area for elastocaloric refrigeration. There are several applications where a more sophisticated cooling system is necessary to prevent the devices' working temperatures from continuously rising. The failure probability of electrical circuits increases exponentially as temperature rises. The previously reviewed elastocaloric devices don't specifically target this field.
- The numerical model and analysis were accurate and comprehensive throughout. The majority of elastocaloric system models that have been created and presented to the scientific community are 1D [28] and there are not published studies that draw broad maps of elastocaloric device performances on a small scale while simultaneously optimizing the geometrical design and operational parameters.

The specifications for electronic cooling depend on the specific requirements of the application and the electronic components involved. Some of the key parameters may include determining the maximum allowable temperature for

electronic components during operation and calculating the amount of heat produced by electronic components, which must be dissipated to prevent overheating. In the specific case under consideration, the cooling of a computer server has been examined, which cannot exceed a temperature of 85 °C and has a power dissipation requirement of approximately 50 W. The values of ΔT (temperature variation) and the cooling powers that the EC device should meet depend on the specific application and cooling requirements. Optimal ΔT values should be at least 10 K. A computer server typically uses a system of fans and a bulky finned structure to dissipate heat. The term 'ultrasmall' implies that the device is extremely small in size compared to those commonly used for these applications. The reduced size can be advantageous in terms of space and weight.

Design of the CHECK TEMPERATURE Architecture

The issue of cooling electronic circuits represents a crucial challenge in the design and operation of advanced electronic devices. Electronic circuits generate heat during their operation due to electrical resistance in components, energy losses, and other intrinsic processes related to device functioning. Excessive temperatures can lead to various problems: at high temperatures, the electrical conductivity of some materials may decrease, causing a reduction in circuit efficiency; elevated temperatures can accelerate the degradation of materials and solder joints, reducing the overall lifespan of the device; at high temperatures, certain components may become unstable, causing malfunctions and unpredictable circuit behavior; the resistance of conductors increases with temperature, leading to greater energy dissipation in the form of heat. Effective cooling solutions are required to address these issues. To design CHECK TEMPERATURE, the study first compares two different configurations for system design: one bending-based and one tensile-based. It is targeted to satisfy the application of electronic circuits cooling. An example of an electronic device that may need to dissipate around 50 watts of heat could be a high-end server or an intensive processing system, such as a data processing server or a 3D graphics rendering server. These types of devices often contain powerful processors, graphics processing units (GPUs), and other high-performance components that generate a significant amount of heat during their operation.

The Device Configuration Based on Tensile Loading

Figure 1a shows the design of the layout system. In the left and right SMA beds, respectively, are two locations for the $Ni_{50.8}Ti_{49.2}$ wires. Each regenerator has two hollow support structures into which the wires are attached. The two middle supports are pulled by a hydraulic piston, and the load is then transferred to the $Ni_{50.8}Ti_{49.2}$ wires. The left and right SMA beds were both set to 50% maximum strain under equilibrium conditions as a result of the system's symmetrical design, which allowed the work recovery function to increase system effectiveness. The left SMA bed could be loaded automatically using the unloading force when the right SMA bed was discharged from the 100% maximum strain back to the equilibrium strain. Due to the residual stress from the left/right SMA bed, the force supplied by the pistons might be decreased from the equilibrium strain condition to the strain-free state. The wires have a diameter of 0.5 mm and are 300 mm long. To avoid the leakage phenomenon that could harm the prototype's mechanical component, air was chosen as the HTF. Additionally, the air offers simpler mechanical design and easier handling. On the left and right sides, there are two air inlet and outflow ducts. A temperature profile along the duct is caused by the cyclical traction (loading) and relaxation (unloading) of the wires, allowing for a continuous flow of cold and hot air that might be supplied directly to the electronic equipment to be refrigerated.

The Device Configuration Based on Loading Through Bending

The bending-based prototype comprises two miniature channels (an upper and a lower one) where wires made of elastocaloric materials are placed along the direction of the HTF; the wires are secured to the extremities through bars. The two channels are separated by a lengthy bar system. A bending plate is positioned in the middle of the channels, and as Fig. 1b explains in more depth, it oversees the loading and unloading of the wires due to the bending operation produced by up and down movements. When the elastocaloric material is loaded, HTF (air) flows through the channels and releases heat; when the eC material is unloaded, it absorbs heat through the HTF flowing in the opposite direction. The inner wires should be put in an unloaded position in the downer channel at the same time, and the air should flow in the opposite direction to transfer heat to the SMA wires. Additionally, the device behaves in the opposite manner as the plate goes downward: the wires in the top channel become unloaded while those in the lower channel become loaded. By doing this, the refrigeration cycle's beneficial effect can be attained at double frequency with respect to the operations of a single AeR regenerator. As first design prescription, 240 $Ni_{50.8}Ti_{49.2}$ [36] alloy wires ($D = 0.5$ mm; $L = 0.3$ m each, for a total mass of 61 g) are intended to be mounted in the device. $Ni_{50.8}Ti_{49.2}$ was chosen because of its Austenite Finish (A_F) temperature (that determines the

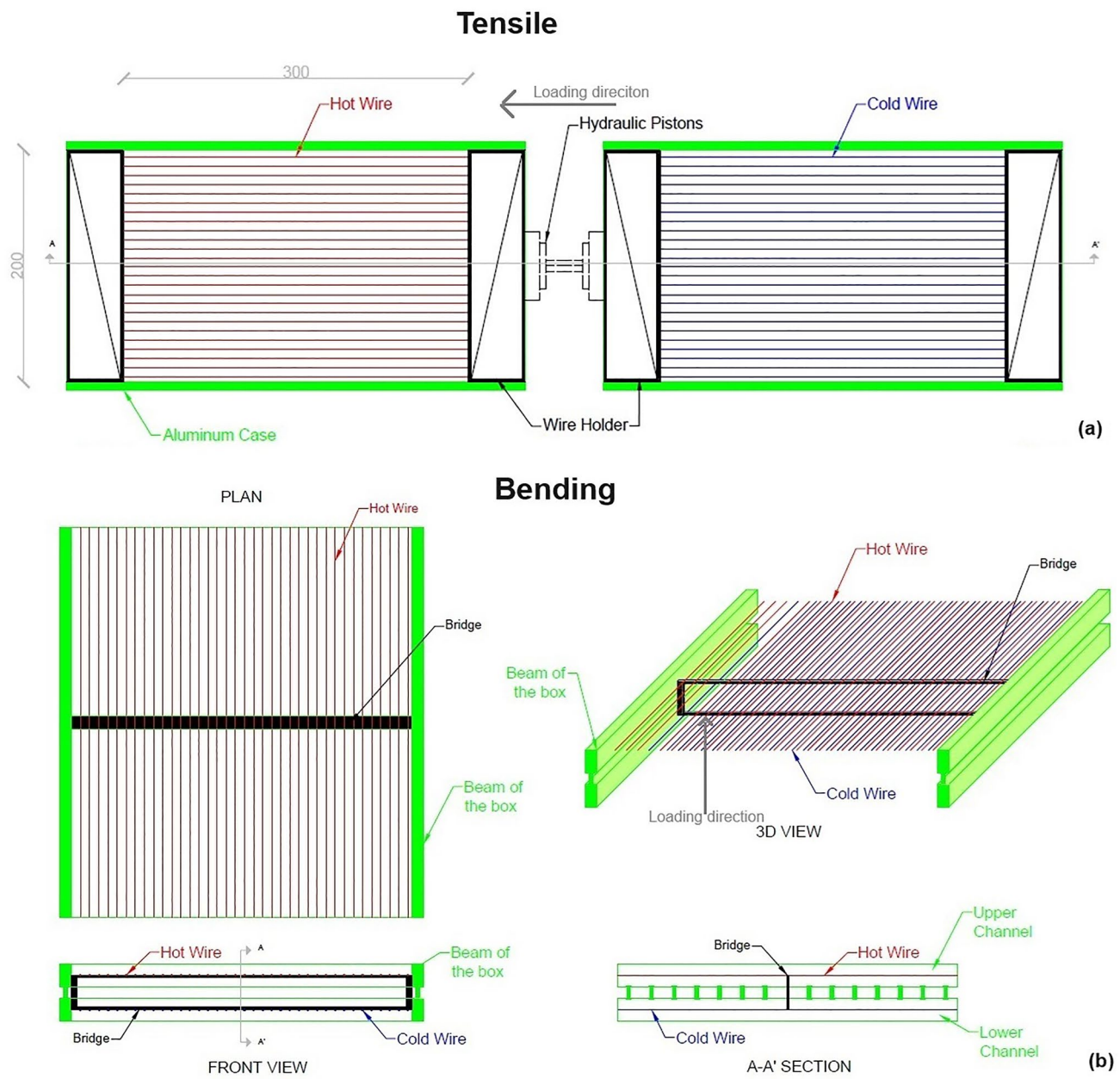

Fig. 1 Layout of **a** tensile and **b** bending configurations

most suitable temperature range) since room temperature was intended to be the operating range for the device.

The Numerical Model

The CHECK TEMPERATURE device was designed and numerically tested using the same mathematical model in both the tensile and bending configurations. The temperature distribution in the cross section is regarded as negligible in this model due to the thin channel walls. As a result, the model is 2D, and the temperature distribution has been assessed in both the x (direction of air flow) and y directions. With the following simplification, the model reproduces all four AeR cycle phases. The following factors are assumed: (1) the elastocaloric material is isotropic with respect to thermal conductivity; (2) the irradiation heat transfer mechanism is not taken into account; (3) the device is deemed adiabatic with respect to the external ambient; (4) the viscous dissipation term in the energy equation of air is omitted.

The ruling equations are:

$$\begin{cases} \frac{\partial u}{\partial x}+\frac{\partial v}{\partial y}=0 \\ \frac{\partial u}{\partial t}+u\frac{\partial u}{\partial x}+v\frac{\partial u}{\partial y}=-\frac{1}{\rho_{air}}\frac{\partial p}{\partial x}+\nu\left(\frac{\partial^2 u}{\partial x^2}+\frac{\partial^2 u}{\partial y^2}\right) \\ \frac{\partial v}{\partial t}+u\frac{\partial v}{\partial x}+v\frac{\partial v}{\partial y}=-\frac{1}{\rho_{air}}\frac{\partial p}{\partial y}+\nu\left(\frac{\partial^2 v}{\partial x^2}+\frac{\partial^2 v}{\partial y^2}\right) \\ \frac{\partial T_{air}}{\partial t}+u\frac{\partial T_{air}}{\partial x}+v\frac{\partial T_{air}}{\partial y}=\frac{k_{air}}{\rho_{air}c_{air,p}}\left(\frac{\partial^2 T_{air}}{\partial x^2}+\frac{\partial^2 T_{air}}{\partial y^2}\right) \\ \frac{\partial T_{SMA}}{\partial t}=\frac{k_{SMA}}{\rho_{SMA}c_{SMA,p}}\left(\frac{\partial^2 T_{SMA}}{\partial x^2}+\frac{\partial^2 T_{SMA}}{\partial y^2}\right)+g''' \end{cases} \tag{1}$$

where g''' takes into account the eCE and represents a heat source during the loading phase of the AeR cycle and a sink during the unloading process. Since the stress is constant during the fluid flow processes (II and IV process), the g'''' component is not considered in the solid energy equation (in other words it is equal to zero). The equations of continuity of the mass and the balancing equations of momentum of the fluid are not taken into account during loading and unloading steps (I and III processes) since the fluid velocity is zero. Convective components in the fluid energy balance equation are not even taken into account throughout these two phases. The g'' is positive during loading, whereas it is negative when unloading and it has the following equation:

$$g''' = g_{load} * an_1(t) + g_{unload} * an_2(t) \tag{2}$$

where $an_1(t)$ and $an_2(t)$ are two analytical functions reproducing two square waves functions, whose amplitude can be valuated as:

$$g_{load} = \rho_{SMA}\left(\Delta H_{load} + w_{load}\right)\dot{\xi}_M \tag{3}$$

$$g_{unload} = \rho_{SMA}\left(\Delta H_{unload} + w_{unload}\right)\dot{\xi}_M \tag{4}$$

By adopting variable values of latent heat for loading and unloading, as well as the necessary effort, the thermal hysteresis of the SMA is not directly modeled but estimated [37]. Tusek et al. [38] state that the area contained by the hysteresis cycle created by the transformations in the s-T plane can be used to estimate the net-work as follows:

$$w_{net} = w_{load} - w_{unload} \tag{5}$$

The martensite volume fraction $\dot{\xi}_M$ is evaluated through Eq. (6):

$$\dot{\xi}_M = -\xi_M \psi^{MA}\left(T_{SMA},\sigma\right) + \xi_A \psi^{AM}\left(T_{SMA},\sigma\right) \tag{6}$$

during the A-M and the M-A transformations:

$$\xi_A + \xi_M = 1 \tag{7}$$

The transition probabilities ψ^{MA} and ψ^{AM} are calculated through the approach proposed by Qian et al. [39]:

$$\psi^{AM}\left(T_{SMA},\sigma\right) = \frac{1}{\theta}\frac{\exp\left(-a\left(\frac{\sigma_{AM}(T_{SMA})-\sigma}{E_A}\right)^2\right)}{\mathrm{erf}\left(\sqrt{a}\frac{\sigma_{AM}(T_{SMA})-\sigma}{E_A}\right)+\mathrm{erf}\left(\sqrt{a}\frac{\sigma_{AM}(T_{SMA})+\sigma}{E_A}\right)} \tag{8}$$

$$\psi^{MA}\left(T_{SMA},\sigma\right) = \frac{1}{\theta}\frac{\exp\left(-b\left(\frac{\sigma_{MA}(T_{SMA})-\sigma}{E_M}\right)^2\right)}{\mathrm{erfc}\left(\sqrt{b}\frac{\sigma_{MA}(T_{SMA})-\sigma}{E_M}\right)} \tag{9}$$

where:

$$a = \frac{E_A V_{SMA}}{2BT_{SMA}} \tag{10}$$

$$b = \frac{E_M V_{SMA}}{2BT_{SMA}} \tag{11}$$

The binary alloy $Ni_{50.8}Ti_{49.2}$ [36] subjected to treatments to achieve a longer fatigue life is the SMA used in this study. Table 1 lists the thermophysical characteristics.

For loading and unloading cycles, 8% strain at a strain rate of 0.025 s^{-1} is taken into account. It is decided to load and unload for 0.2 s, time interval ensuring the transformation would be adiabatic.

The Finite Element Method (FEM) is used to solve the model, which is run through the software COMSOL Multiphysics. The domain has been divided into triangular elements in accordance with the FEM technique. This division was made after free triangular meshing.

The FEM model's equations were solved using a time-dependent solver that used the implicit Backward Differentiation Formula (BDF) as a time-step method.

Until a steady state is reached, the four AeR cycle stages are repeated in sequences of four time-dependent sequential steps. Every step's starting condition is the preceding step's final condition. Until the cyclicity criteria is met at

Table 1 Thermophysical characteristics of binary NiTi alloy

Property	Value	Unit
Af	− 14.5	°C
As	− 25.5	°C
Mf	− 38.1	°C
Ms	− 51.2	°C
k_{SMA}	15	W m^{-1} K^{-1}
ρ_{SMA}	6500	kg m^{-3}
c_{SMA}	550	J kg^{-1} K^{-1}
$\Delta H_{load,tensile}$	12	J g^{-1}
$\Delta H_{unload,tensile}$	9.4	J g^{-1}
$\Delta H_{load,bending}$	7.2	J g^{-1}
$\Delta H_{unload,bending}$	6.1	J g^{-1}

every location in the domain, the following procedures are repeated:

$$\delta = max\left\{T\left(x,y,0+nt_{cycle}\right) - T\left(x,y,t_{cycle}+nt_{cycle}\right)\right\} < \overline{\varepsilon} \tag{12}$$

For the solver of the introduced model, the absolute and relative tolerances are set at 5×10^{-4} and 1×10^{-2}, respectively.

Through the use of several grids with identical beginning, boundary, and operating circumstances, simulations were run to examine the solution's independence from the spatial grid. The domain was divided into 81,218 volume triangle components for the coarse grid, 137,084 elements for the normal grid, and 384,424 volume elements for the dense grid. We observed a fair agreement between the solution using 137,084 and 384,424 (maximum difference between air temperatures lower than 0.03 K) with respect to the temperature profiles in the last stage of the AeR cycle. As a result, we have decided to work with a normal grid (137,084 volume triangular components) in order to reduce the calculation time.

The model has been experimentally validated as extensively reported by a previous investigation on the introduced model (see "Results and discussion" section of reference [40]).

Results and Discussion

Campaign of Simulations n° 1: Bending vs Tensile AeR Configuration

The first set of simulations [40] was run on both the regenerator configurations (bending and tensile) while 120 per channel are the elastocaloric thin wires ($D = 0.5$ mm; L = 30 cm) under the following operating conditions:

- Variable velocity of the air entering the device: 3,5,7,9,11 m s^{-1}.
- Fixed temperature of the air entering the device: 293 K.
- 0.2 s is the time for loading and unloading steps whereas variable is the time for air flowing steps in the AeR cycle: from 4 to 12 s each, i.e. variable frequency of the AeR cycle.

The following thermal and energy performance of the two configurations of the device are estimated:

$$\Delta T_{span} = \left(T_{env} - \frac{1}{t_{cycle}}\int_{0+nt_{cycle}}^{t_{cycle}+nt_{cycle}} T_{air,outlet}(t)dt\right) \tag{13}$$

$$\dot{Q}_{cool} = \frac{1}{t_{cycle}}\int_{t_{load}+t_{fluid}+t_{unload}+nt_{cycle}}^{t_{cycle}+nt_{cycle}} \dot{m}_{air}c_{air}\left(T_{env} - T_{air}(0,y,t)\right)dt \tag{14}$$

$$COP = \frac{\dot{Q}_{ref}}{\dot{W}} \tag{15}$$

The temperature span is measured as the difference, time-averaged over a full cycle, between the air temperature at the inlet and the air temperature exiting the cold side of the regenerator. On the cold side of the regenerator, the cooling power is responsible for the integral in the time of the air temperature variation.

The cooling power to global work per unit time ratio is known as the COP. The mechanical power associated with the air flow's motion (as determined by pressure losses) and the loading of the wires (as determined by the tensile work recovery) is considered in the global work.

Figure 2 shows the temperature span for the two geometries [(a) tensile, (b) bending] as a function of fluid flowing time for parametrized air velocity. The two geometries exhibit quite distinct behaviors: for each velocity, the temperature range of tensile is an increasing function of fluid flow duration, but under bending, it reaches a maximum and subsequently drops. We discovered that the SMA's ΔT_{ad} is larger with tensile than with bending (17 K vs. 11 K in unloading) based on experimental findings and conclusions from the numerical model. As a result, in the tensile configuration air needs more time to remove the thermal load from the wires due elastocaloric effect.

Since it is impossible to test a flow time higher than 12 s because it would be equivalent to a cycle frequency that is too low, we are still a long way from the point where decreasing the temperature difference between wire and air reduces the effectiveness of the heat exchange. Conversely, when the contact time grows over 8–10 s during the bending, the wires become extremely close to the air temperature, reducing the temperature range and increasing the efficiency of the heat exchange. As a result, there is an ideal fluid blowing time for each fluid velocity that maximizes the temperature range. At low fluid blowing, the temperature spans achieved with the two systems are comparable.

The temperature range of the tensile is greater for long times (12 s), reaching a maximum increase of 9 K at v = 3 m s^{-1}. The temperature range rises at a constant time as the air velocity falls. In fact, slowing down lengthens the time that air spends being heated by the elastocaloric wires. For tensile configuration tested at at 3 m s^{-1} with a fluid blown duration of 12 s, the maximum temperature span is 9 K, but for bending at 3 m s^{-1} with a period of 8 s, it is 7.2 K.

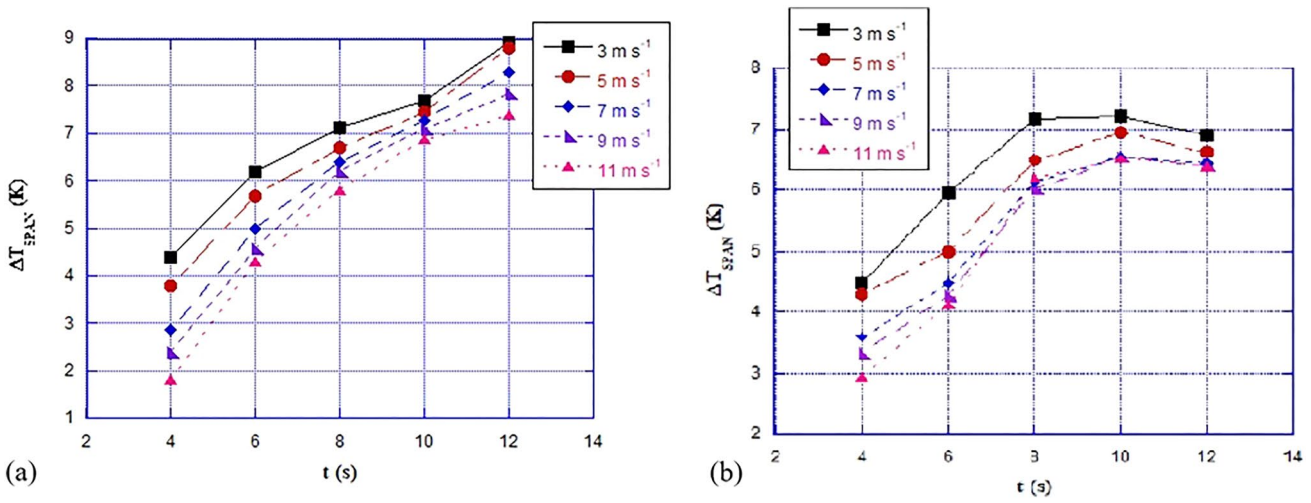

Fig. 2 Temperature span vs time for fluid flow parametrized for air velocity: **a** tensile load; **b** bending

The cooling power for both configurations: (a) tensile, (b) bending is presented in Fig. 3 as a function of fluid blown time parametrized for fluid velocity. Since the mass flow rate likewise rises, the cooling load at a given time is an increasing function of air velocity. Because cooling power is maximized at maximum velocity and temperature span is maximized at minimum velocity, there is a trade-off between the two. The cooling power for each velocity in the tensile design increases as the flowing time increases. In contrast, the cooling power for bending-based design reaches its maximum in accordance with the maximum temperature range. At the lowest fluid blowing velocity, the cooling power of the two systems is comparable.

For all the other investigated time values the tensile cooling powers are always better, reaching the maximum deviation (+30% mean value) at the maximum passage time (12 s). The maximum cooling power is 76 W for tensile at 12 s and 65 W for bending at 10 s with an air velocity of 11 m s^{-1}.

The tensile cooling capabilities are always superior for all other studied time values, reaching the maximum deviation (+30% mean value) at the maximum passage time (12 s). With an air velocity of 11 m s^{-1}, the maximum cooling power is 76 W for tensile at 12 s and 65 W for bending at 10 s. Figure 4 shows the COP for both the topologies: (a) tensile; (b) bending, as a function of air velocity

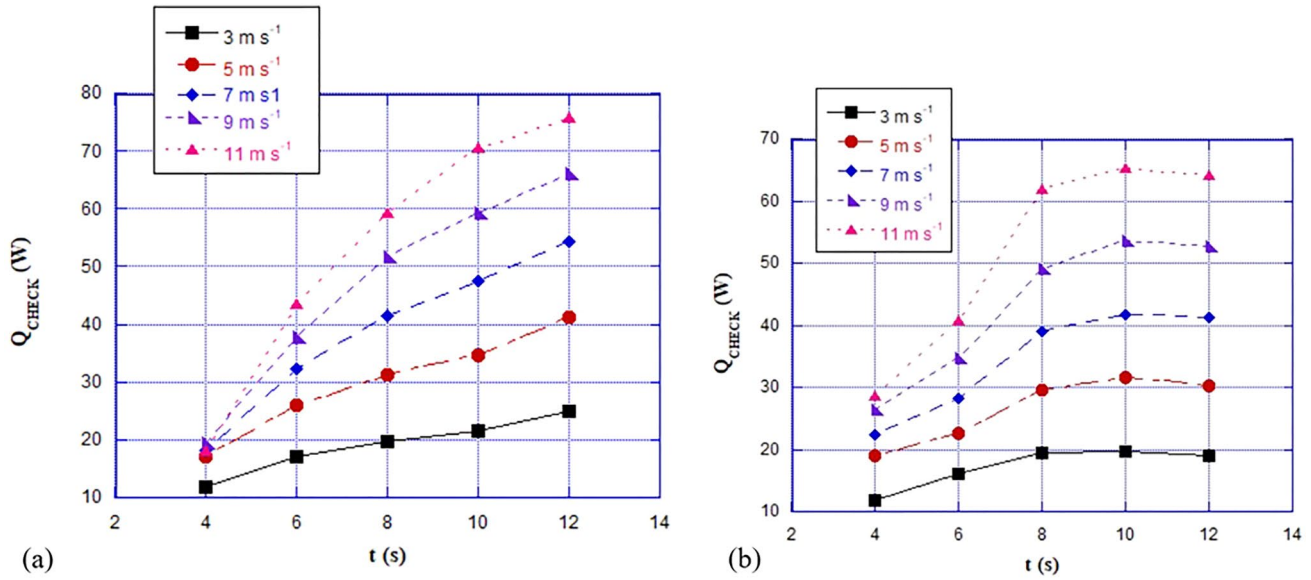

Fig. 3 Cooling power vs time for fluid flow parametrized for air velocity: **a** tensile load; **b** bending

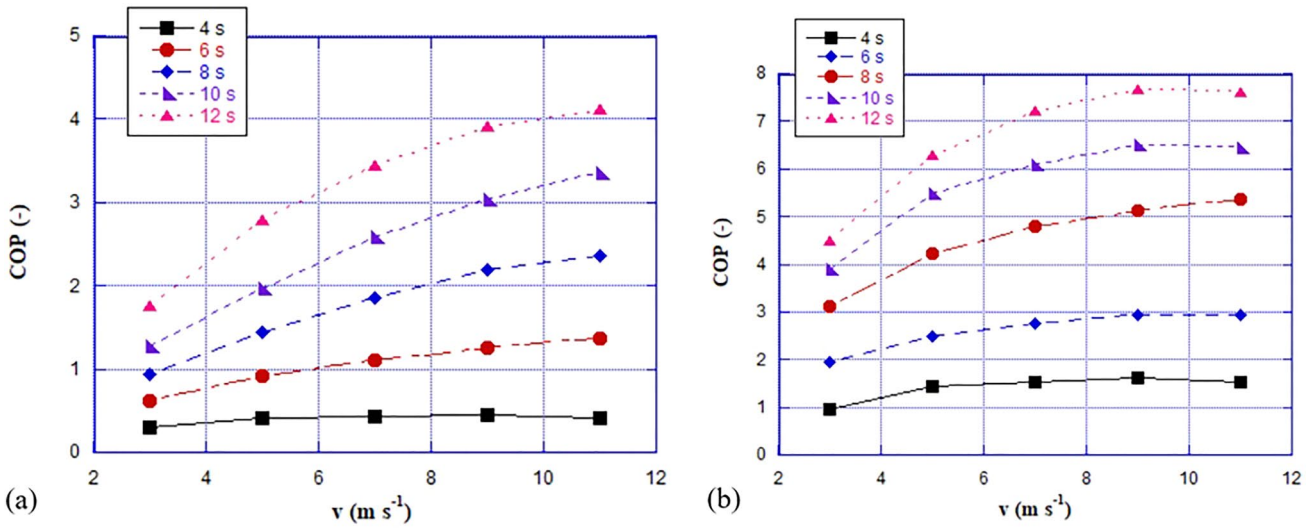

Fig. 4 COP vs time for fluid flow parametrized for air velocity: **a** tensile load; **b** bending

parametrized for blowing time. Since the work per time unit varies very slightly (the loading of the wires is the main contributor), and the cooling power grows with the flow rate, COP in the tensile device (Fig. 7a) is an increasing function of the velocity at fixed time.

On the other hand, the COP of the bending device reaches a maximum of around 9 m s^{-1}. At constant velocity, both the cooling power and COP rise with time. The eC system can only function at a lower limit with COP values of less than 3, as these values have been tested for times shorter than 6 s. Because less work is required to load the wires in the tensile test than in the bending test (from a minimum of + 46% to a maximum of + 77%), the bending device's COP is consistently greater than the tensile test's. Based on bending at 9 m s^{-1} air velocity and 12 s fluid blowing duration, the device's best COP is 7.7; for tensile at 11 m s^{-1} and 12 s, it is 4.15.

The considerations emerging from this first investigation are:

- At moderate fluid flow times, the temperature range attained by the two systems is comparable.
- The temperature span of the tensile is greater than the temperature span of the bending at high time (12 s), reaching a maximum rise of 2 K at v = 3 m s^{-1}.
- At an air velocity of 3 m s^{-1}, or 9 K for tensile with a fluid blowing time of 12 s and 7.2 K for bending with a period of 8 s, the maximum temperature span has been reached.
- At the lowest fluid flowing time of 4 s, the cooling power of the two arrangements is comparable.
- The tensile cooling powers are consistently improved for all other passage periods, reaching the largest divergence (+ 30% mean value) at the longest possible passage time (12 s).
- At an air velocity of 11 m s^{-1}, or 76 W with tensile at 12 s and 65 W with bending at 10 s, the maximum cooling power is achieved.
- The system can only function at a lower limit with COP values of less than 3, as these values have been tested for times shorter than 6 s.
- The device's COP based on bending is consistently greater (ranging from a minimum of + 46% to a maximum of + 77%) in all tests than the device based on tensile, since the latter requires a substantially smaller amount of work to load the wires than the former.
- The device's best COP of 7.7 for bending at 9 m s^{-1} air velocity and 4.15 for tensile at 11 m s^{-1} has been achieved during a fluid flowing period of 12 s.

Thus, it is feasible to conclude from the results that the most promising configuration is based on bending, a design choice resulting appropriate for cooling the electronic circuits.

Campaign of Simulations n° 2: the Influence of Distances on Bending Regenerator

After having asserted that bending regenerator is the choice, the second campaign of simulations [41] has the aim to well define the optimal combinations of geometrical parameters and operative conditions. Indeed, both of them are varied and the deriving energy performances are calculated and examined.

The distance *d* stacked between the positioning of two consecutive wires along the device's channels has been the

first geometrical parameter to be studied. First, the influence of two distinct distances ($d = 0.5$ mm and $d = 1.2$ mm) on the energy performances of the device have been taken into consideration at a fixed length of the wire (20 cm).

Figure 5 depicts the temperature span global ($\Delta T_{\text{span,global}}$) vs frequency of the device (f). The *temperature span global* accounts for the global span on the temperatures of the air between the hot flux and cold flux exiting from the device, in an entire cycle.

and it is estimated as:

$$\Delta T_{span,global} = \left(\frac{1}{t_{cycle}} \int_{t_{load}+nt_{cycle}}^{t_{load}+t_{fluid}+nt_{cycle}} T_{air}(L,y,t)dt - \frac{1}{t_{cycle}} \int_{t_{load}+t_{fluid}+t_{unload}+nt_{cycle}}^{t_{cycle}+nt_{cycle}} T_{air}(0,y,t)dt \right) \quad (16)$$

There is always a perfect frequency that maximizes the temperature gap for fixed velocity and distance.

If the wires are positioned with $d = 0.5$ mm, under identical operating conditions, with peaks at 0.122 Hz for each tested v and an absolute maximum of 23.9 K with a velocity of 3 m s^{-1}, the measured $\Delta T_{\text{span,global}}$ are bigger.

If there is 1.2 mm between the wires, changing the velocities causes the maximum to fall at various frequencies. The highest possible global temperature span is 20.1 K, measured at 0.239 Hz, and 3 m s^{-1}. One can estimate a medium increment of + 55% for the $\Delta T_{\text{span,global}}$ depicted in Fig. 5a by comparing the two geometric configurations.

The cooling capacity of the device is shown in Fig. 6 as a function of frequency parametrized for air velocity, with the wires spaced at (a) 0.5 mm and (b) 1.2 mm, respectively. Because of the increased fluid flow rate with increasing velocity values, the more is v, the higher are the cooling power values. If the velocity is fixed, $\dot{Q}_{cool}$ peaks at frequencies other than those of temperature span, indicating a trade-off between maximizing ΔT_{span} and $\dot{Q}_{cool}$. With $d = 0.5$ mm and 1.2 mm, the highest $\dot{Q}_{cool}$ evaluated are 68.1 W and 49.0 W at 0.096 Hz and 11 m s^{-1}, respectively. For the geometry with $d = 0.5$ mm, the comparison between the two configurations identifies a medium augmentation in cooling power of + 30%.

In Fig. 7a and b, the COP is displayed as a function of the cycle frequency parametrized for air velocity.

Except for very low frequency values, the COP at fixed frequency increases with air velocity, reaching maximum values of 6.8 ($v = 9$ m s^{-1}; $f = 0.096$ Hz) and 5.2 ($v = 7$ m s^{-1}; $f = 0.096$ Hz) for $d = 0.5$ mm and $d = 1.2$ mm, respectively. At constant speed, the COP falls off as the cycle frequency rises. The acceptable threshold value, 3, is the range above which the test gadget is expected to function. Given the length of time required to achieve a complete convective heat exchange between the wires and air, the device must operate at a lower frequency.

Convective heat transfer takes longer when cycle frequencies are smaller. However, given that the geometry with wires spaced at 0.5 mm consistently outperforms the 1.2 mm configuration by + 30%, it can be seen from the figures that, when always using 3 as the threshold value, the former (d = 0.5 mm) allows the device to operate up to higher frequencies (0.161 Hz), as opposed to the latter (1.2 mm), where the limit is 0.122 Hz.

The device mounting wires with a length of 20 and0 cm stacked at a distance of 0.5 mm worldwide confers greater

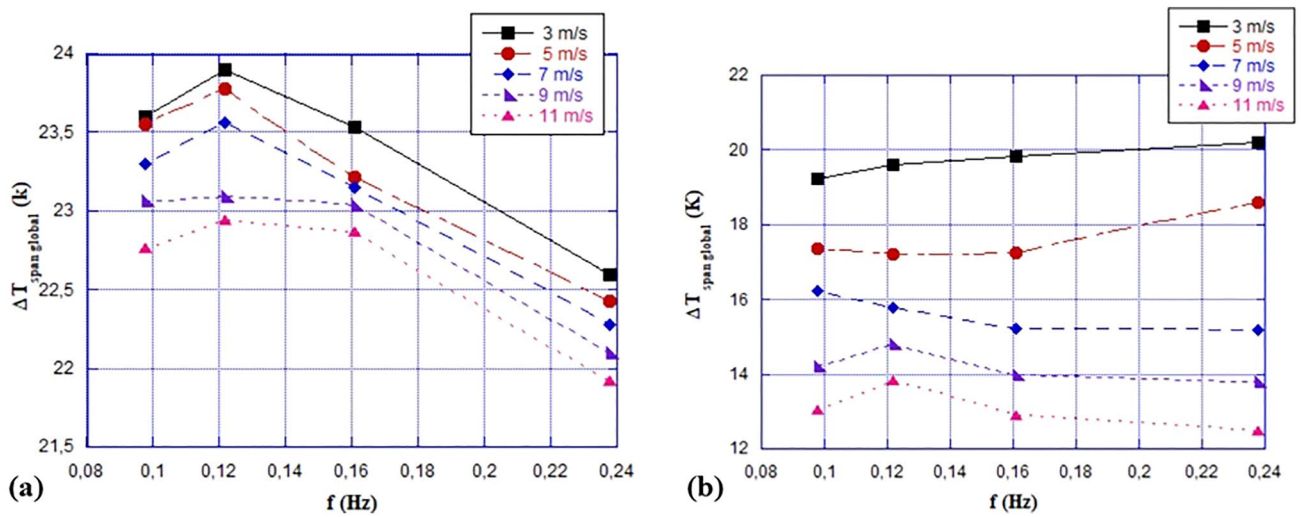

Fig. 5 Temperature span global vs frequency of the device parametrized for air velocity for wires placed at: **a** 0.5 mm; **b** 1.2 mm

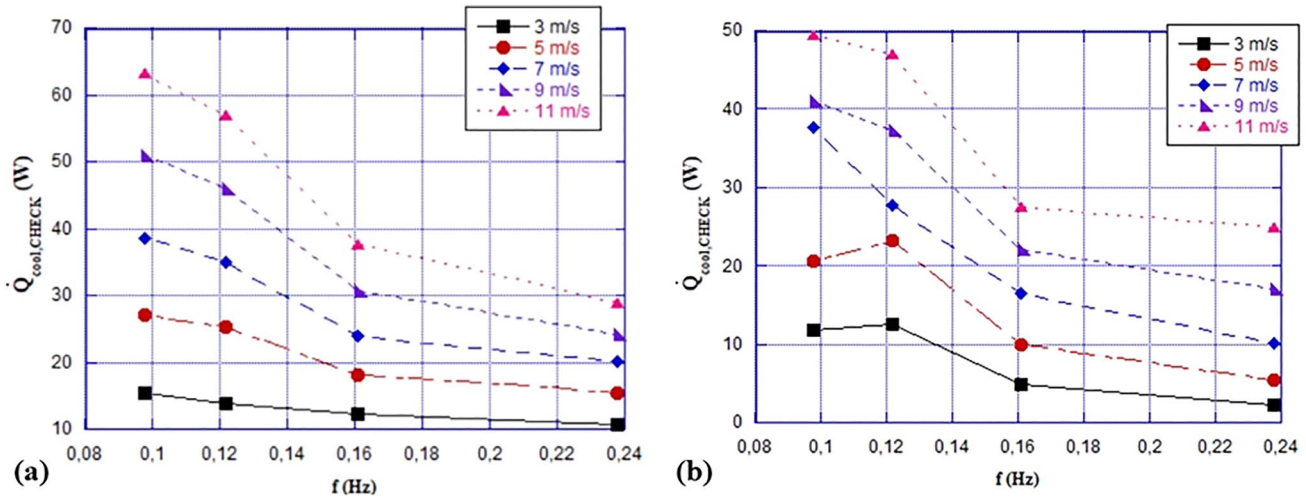

Fig. 6 Cooling power vs frequency of the device parametrized for fluid velocity for wires placed at: **a** 0.5 mm; **b** 1.2 mm

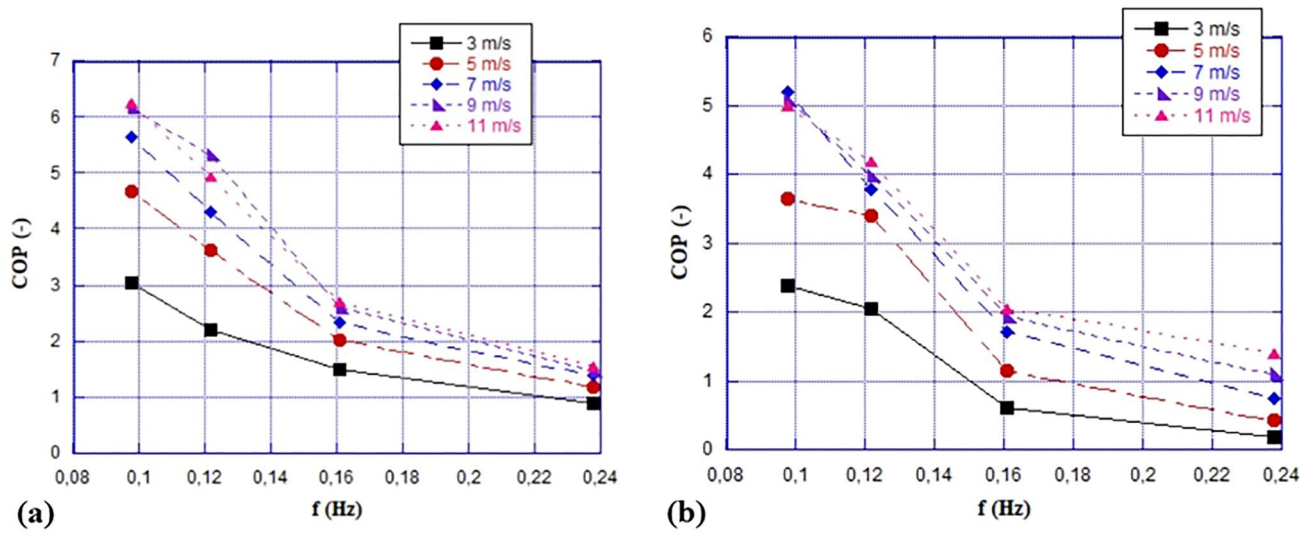

Fig. 7 COP vs frequency of the device parametrized for fluid velocity for wires placed at: **a** 0.5 mm; **b** 1.2 mm

energy performances in terms of temperature span, cooling power, and COP, based on all the analysis done.

Campaign of Simulations n° 3: the Influence of Wire Length on Bending Regenerator

In the third phase of the study [41], wires with lengths of 20 cm and 30 cm are compared, taking into account equal numbers of wires (240). This results in varying masses of the elastocaloric material used in the device, which are 61.23 g and 91.85 g, respectively, for lengths of 20 cm and 30 cm.

Figure 8 shows the temperature span ($d = 0.5$ mm) as a function of time for the two geometries where (a) $L = 20$ cm, (b) $L = 30$ cm. The two geometries exhibit distinct behaviors, as seen in the figures: the temperature span of the $L = 20$ cm design increases with fluid flow time for all velocities, the same trend is possible to observe for the longer wires ($L = 30$ cm). The temperature span is slightly, but not noticeably, affected by the length increase because the values are similar (+4% as a medium increment).

The cooling power is plotted in Fig. 9 as a function of air flow time, parametrized for v and with wire lengths of (a) $L = 20$ cm and (b) $L = 30$ cm. Since the mass flow rate likewise increases with air velocity, the cooling power increases with equal frequency, or air flow time. Consequently, once more, there is a trade-off between cooling power and ΔT_{SPAN}. While $\dot{Q}_{cool}$ for the design with $L = 20$ cm grows with air flow time, it peaks at the same frequency as the peak

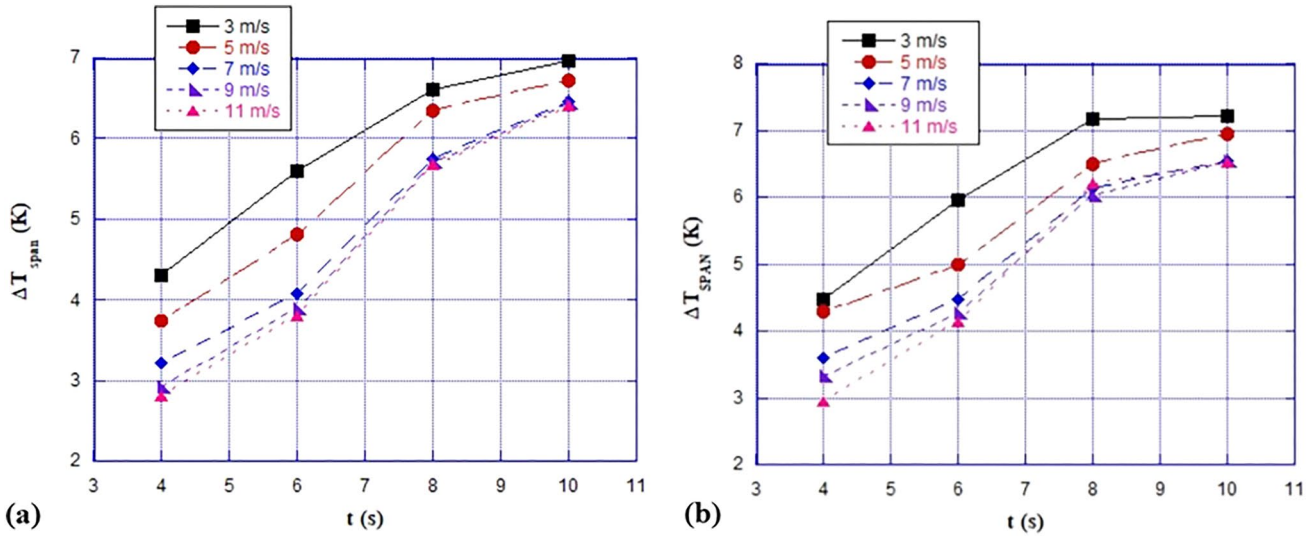

Fig. 8 Temperature span on cold vs time for fluid flow parametrized for air velocity for wires length of: **a** 20 cm; **b** 30 cm, with $d = 0.5$ mm

of ΔT_{SPAN} for $L = 30$ cm. The computed variances became less at higher frequencies (the smallest being a + 10% mean value at $f = 0.238$ Hz, or 4 s for air flow time). + 20% is the maximum increment that has been evaluated for $f = 0.098$ Hz (10 s as air flow time).

The coefficient of performance versus fluid flow speed parametrized for the fluid time for (c) $L = 20$ cm and (d) $L = 30$ cm wire lengths is displayed in Fig. 9c and d. The COP for both designs under investigation increases as air flow speed increases, just as it does for cooling power. This is because the mechanical power required for wire loading dominates the fluid motion contribution to total work per unit time. While the former is fixed, the latter depends on air speed. Furthermore, for a given fluid flow rate, COP values increase with cycle time.

The COP for the $L = 30$ cm configuration, which ranges from a minimum of + 11% to a maximum of + 46%), is always greater than $L = 20$ cm in all working points. The time for fluid to flow must always be more than 6 s in order for the device to operate in working points with acceptable COP (not less than 3). The largest COPs are determined for t = 10 s and high velocities (9 m s^{-1} and 11 m s^{-1}); in fact, the COP values fall between 6.0 and 6.5 in these operating conditions.

Conclusion

In this study, CHECK TEMPERATURE, a 2D numerical model is used to investigate the design of the first elastocaloric device for cooling electronic circuits. The following conclusions from the investigation's findings can be summed up as follows:

- When it comes to the tensile arrangement, bending is the preferable option, according to the consideration of "Campaign of simulations n° 1: bending vs tensile AeR configuration" section;
- Wires stacked at 0.5 mm along the channel ensures higher values of temperature span, cooling power and COP.
- The time required for fluid to flow must always be longer than 6 s in order for the device to operate in working points with acceptable COP (not less than 3). The highest COPs are estimated for t = 10 s and high velocities (9 m s^{-1} and 11 m s^{-1}), with values falling within the range of 6.0–6.5.
- With the number of wires in the device (240) remaining constant, the L = 20 cm configuration uses 61.23 g of elastocaloric material while the L = 30 cm configuration uses 91.85 g.

Based on the previously mentioned points, it is clear that $d = 0.5$ mm is the ideal distance to arrange the wires among the objects under investigation. Additionally, although if the energy performance of the solution with wires 30 cm long is slightly higher, the solution with wires 20 cm long must be preferred because 30% less elastocaloric material is utilized, resulting in a cost savings.

The gathered and discussed results support the viability of using elastocaloric technology in the area of cooling electronic circuits. The device is now being built, and the ideal geometrical design conditions have been found. The next aspect of the upcoming research will be the comparison of experimental data provided by the CHECK TEMPERATURE device with numerical results. The model will be helpful in identifying further areas for the experimental device's improvement.

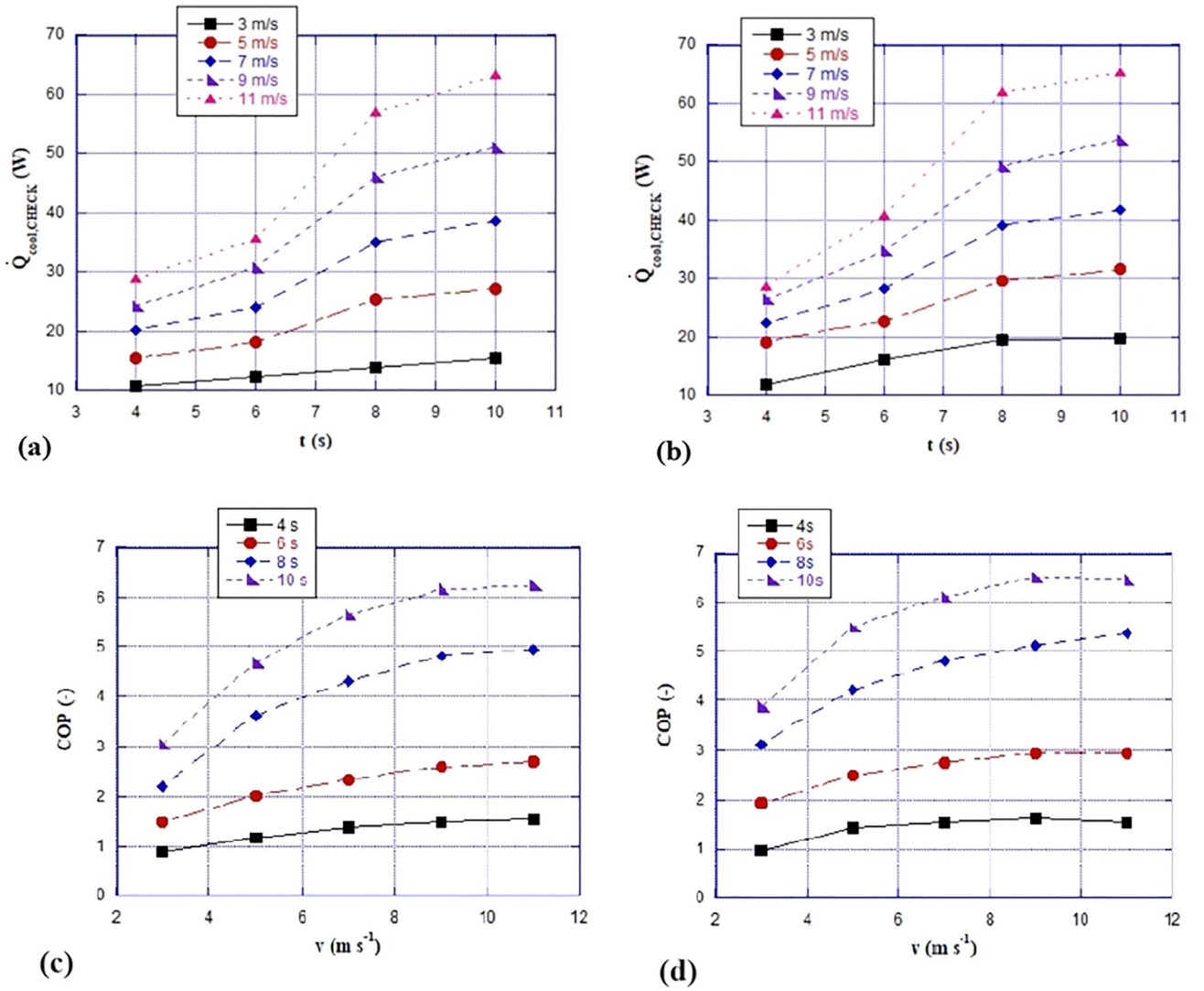

Fig. 9 Cooling power and COP vs time for fluid flow parametrized for fluid velocity for wires length

Acknowledgements The paper is realized from the project CHECK TEMPERATURE that is financially supported by the 2021 internal grant reserved for Fixed-Term Research of Department of Industrial Engineering, University of Naples Federico II.

Funding Open access funding provided by Università degli Studi di Napoli Federico II within the CRUI-CARE Agreement.

Open Access This article is licensed under a Creative Commons Attribution 4.0 International License, which permits use, sharing, adaptation, distribution and reproduction in any medium or format, as long as you give appropriate credit to the original author(s) and the source, provide a link to the Creative Commons licence, and indicate if changes were made. The images or other third party material in this article are included in the article's Creative Commons licence, unless indicated otherwise in a credit line to the material. If material is not included in the article's Creative Commons licence and your intended use is not permitted by statutory regulation or exceeds the permitted use, you will need to obtain permission directly from the copyright holder. To view a copy of this licence, visit http://creativecommons.org/licenses/by/4.0/.

References

1. Qian S, Nasuta D, Rhoads A, Wang Yi, Geng Y, Hwang Y, Radermacher R, Takeuchi I (2016) Not-in-kind cooling technologies: A quantitative comparison of refrigerants and system performance. Int J Refrig 62:177–192
2. Chen J, Lei L, Fang G (2021) Elastocaloric cooling of shape memory alloys: a review. Mater Today Commun 28:102706
3. Bonnot E, Romero R, Mañosa L, Vives E, Planes A (2008) Elastocaloric effect associated with the martensitic transition in shape-memory alloys. Phys Rev Lett 100(12):125901
4. Yuan L, Wang Y, Yu J, Greco A, Masselli C, Qian S (2023) Numerical study of a double-effect elastocaloric cooling system powered by low-grade heat. Appl Therm Eng 218:119302

5. Zhou M, Li YS, Zhang C, Li LF (2018) Elastocaloric effect and mechanical behavior for NiTi shape memory alloys. Chin Phys B 27(10):106501
6. Zhang J, Zhu Y, Cheng S, Yao S, Sun Q (2022) Enhancing cooling performance of NiTi elastocaloric tube refrigerant via internal grooving. Appl Therm Eng 213:118657
7. Mosca HO, Bozzolo G, Del Grosso MF (2012) Atomistic modeling of ternary additions to NiTi and quaternary additions to Ni–Ti–Pd, Ni–Ti–Pt and Ni–Ti–Hf shape memory alloys. Physica B 407(16):3244–3247
8. Chluba C, Ge W, Lima de Miranda R, Strobel J, Kienle L, Quandt E, Wuttig M (2015) Ultralow-fatigue shape memory alloy films. Science 348(6238):1004–1007
9. Bennacer R, Liu B, Yang M, Chen A (2022) Refrigeration performance and the elastocaloric effect in natural and synthetic rubbers. Appl Therm Eng 204(5):117938
10. Daniel Guyomar D, Li Y, Sebald G, Cottinet PJ, Ducharne B, Capsal JF (2013) Elastocaloric modelling of natural rubber. Appl Therm Eng 57(1–2):33–38
11. Xie Z, Sebald G, Guyomar D (2017) Comparison of elastocaloric effect of natural rubber with other caloric effects on different-scale cooling application cases. Appl Therm Eng 111(25):914–926
12. Greco A, Aprea C, Maiorino A, Masselli C (2019) A review of the state of the art of solid-state caloric cooling processes at room-temperature before 2019. Int J Refrig 106:66–88
13. Cui J, Wu Y, Muehlbauer J, Hwang Y, Radermacher R, Fackler S, Takeuchi I (2012) Demonstration of high efficiency elastocaloric cooling with large ΔT using NiTi wires. Appl Phys Lett 101(7):073904
14. Kabirifar P, Žerovnik A, Ahčin Ž, Porenta L, Brojan M, Tušek J (2019) Elastocaloric cooling: state-of-the-art and future challenges in designing regenerative elastocaloric devices. J Mech Eng 65(11–12):615–630
15. Kirsch S-M, Welsch F, Michaelis N, Schmidt M, Wieczorek A, Frenzel J, Eggeler G, Schütze A, Seelecke S (2018) NiTi-based elastocaloric cooling on the macroscale: from basic concepts to realization. Energ Technol 6(8):1567–1587
16. Bruederlin F, Ossmer H, Wendler F, Miyazaki S, Kohl M (2017) SMA foil-based elastocaloric cooling: From material behavior to device engineering. J Phys D Appl Phys 50(42):424003
17. Bruederlin F, Bumke L, Quandt E, Kohl M (2019) Cascaded Sma-film based elastocaloric cooling. Proceedings of 20th International Conference on Solid-State Sensors, Actuators and Microsystems & Eurosensors XXXIII (TRANSDUCERS & EUROSENSORS XXXIII), pp. 1467–1470
18. Snodgrass R, Erickson D (2019) A multistage elastocaloric refrigerator and heat pump with 28 K temperature span. Sci Rep 9(1):1–10
19. Ossmer H, Chluba C, Kauffmann-Weiss S, Quandt E, Kohl M (2016) TiNi-based films for elastocaloric microcooling—fatigue life and device performance. APL Mater 4(6):064102
20. Chen Y, Wang Y, Sun W, Qian S, Liu J (2022) A compact elastocaloric refrigerator. Innovation. https://doi.org/10.1016/j.xinn.2022.100205
21. Ahčin Ž, Dall'Olio S, Žerovnik A, Baškovič UŽ, Porenta L, Kabirifar P, Cerar J, Zupan S, Brojan M, Klemenc J, Tušek J (2022) High-performance cooling and heat pumping based on fatigue-resistant elastocaloric effect in compression. Joule 6(10):2338–2357
22. Ianniciello L, Bartholomé K, Fitger A, Engelbrecht K (2022) Long life elastocaloric regenerator operating under compression. Appl Therm Eng 202:117838
23. Emaikwu N, Catalini D, Muehlbauer J, Hwang Y, Takeuchi I, Radermacher R (2022) Experimental investigation of a staggered-tube active elastocaloric regenerator. Int J Refrig 153(2023):370–377
24. Cirillo L, Farina AR, Greco A, Masselli C (2022) The optimization of the energy performances of a single bunch of elastocaloric elements to be employed in an experimental device. Therm Sci Eng Prog 27:101152
25. Cirillo L, Greco A, Masselli C (2023) The energy performances of an elastocaloric device for air conditioning through numerical investigation. Appl Therm Eng 236:121517
26. Borzacchiello A, Cirillo L, Greco A, Masselli C (2023) A comparison between different materials with elastocaloric effect for a rotary cooling prototype. Appl Therm Eng 235:121344
27. Cirillo L, Greco A, Masselli C (2023) Analysis of the environmental impact of a heat pump based on the elastocaloric effect. Int J Refrig. https://doi.org/10.1016/j.ijrefrig.2023.10.001
28. Qian S, Geng Y, Wang Yi, Ling J, Hwang Y, Radermacher R, Takeuchi I, Cui J (2016) A review of elastocaloric cooling: Materials, cycles and system integrations. Int J Refrig 64:1–19
29. Xu Z, Li G, Zhou Y, Guo C, Huang Y, Hu X, Zhu Q (2023) Tension-compression asymmetry of nickel-based superalloys: A focused review. J Alloy Compd 945:169313
30. Michaelis N, Welsch F, Kirsch SM, Seelecke S, Schütze A (2019) Resistance monitoring of shape memory material stabilization during elastocaloric training. Smart Mater Struct 28(10):105046
31. Ianniciello L, Bartholomé K, Fitger A, Engelbrecht K (2022) Long life elastocaloric regenerator operating under compression. Appl Therm Eng 202(5):117838
32. Zhang K, Kang G, Sun Q (2019) High fatigue life and cooling efficiency of NiTi shape memory alloy under cyclic compression. Scripta Mater 159:62–67
33. Chen J, Zhang K, Kan Q, Yin H, Sun Q (2019) Ultra-high fatigue life of NiTi cylinders for compression-based elastocaloric cooling. Appl Phys Lett 115(9):093902
34. Qian S, Yuan L, Hou H, Takeuchi I (2018) Accurate prediction of work and coefficient of performance of elastocaloric materials with phase transformation kinetics. Sci Technol Built Environ 24(6):673–684
35. Sharar DJ, Radice J, Warzoha R, Hanrahan B, Smith A (2021) Low-force elastocaloric refrigeration via bending. Appl Phys Lett 118(18):184103
36. Zhou M, Li Y, Zhang C, Li S, Wu E, Li W, Li L (2018) The elastocaloric effect of $Ni_{50.8}Ti_{49.2}$ shape memory alloys. J Phys D Appl Phys 51(13):135303
37. Ossmer H, Lambrecht F, Gültig M, Chluba C, Quandt E, Kohl M (2014) Evolution of temperature profiles in TiNi films for elastocaloric cooling. Acta Mat 81:9–20
38. Tušek J, Engelbrecht K, Mañosa L, Vives E, Pryds N (2016) Understanding the thermodynamic properties of the elastocaloric effect through experimentation and modelling. Shape Memory Superelasticity 2(4):317–329
39. Qian S, Yuan L, Yu J, Yan G (2017) Numerical modelling of an active elastocaloric regenerator refrigerator with phase transformation kinetics and the matching principle for materials selection. Energy 141:744–756
40. Cirillo L, Greco A, Masselli C (2023) Development of an electronic circuit cooling system using elastocaloric effect: a FEM comparison among different configurations. Appl Therm Eng 219:119463
41. Masselli C, Cirillo L, Greco A (2023) Cooling of electronic circuits through elastocaloric solid-state technology: a numerical analysis for the development of the CHECK TEMPERATURE prototype. Appl Therm Eng 230:120729

Publisher's Note Springer Nature remains neutral with regard to jurisdictional claims in published maps and institutional affiliations.